

Structure and Kinematics of the Interstellar Medium in front of SN1987A

Jun Xu and Arlin P.S. Crotts

Department of Astronomy, Columbia University, New York, NY 10027

Received _____; accepted _____

ABSTRACT

High resolution (10 km s^{-1}) [N II] echelle spectra, sampled every 13 arcsec in a $6' \times 6'$ region around SN1987A were obtained on the CTIO 4m telescope. The map shows a complicated velocity structure consistent with that reported previously for the interstellar medium (ISM). Three components, $V_{hel} = 265, 277$ and 285 km s^{-1} were identified as N157C (or the R1170-complex: Xu, Crotts & Kunkel 1995). The radius of this large superbubble was found to expand at 10 km s^{-1} , with a lifetime of 6×10^6 years and a total energy of 3×10^{51} ergs determined from its radius and velocity according to superbubble theory (McCray & Kafatos 1987). The $V_{hel} = 235 \text{ km s}^{-1}$ component corresponds to the near side of 600 pc giant superbubble reported earlier. This bubble is over 10^7 years old, and has blown out of the LMC disk. Two other components, $V_{hel} = 255$ and 245 km s^{-1} are identified as the inner major light echo ring (a double-shell structure) at about 130 pc in front of SN1987A. There are also two high velocity components, 300 and 313 km s^{-1} , which are possibly the far side of a superbubble in which SN1987A exploded. We also noticed that there are two components at 269 and 301 km s^{-1} within $20''$ of SN1987A. These structures are probably due to the emission from the progenitor star's red supergiant wind. We find that the time it took the SN1987A progenitor to move to the current location 300 pc behind N157C is comparable to the age of N157C as well as that of the progenitor itself.

Subject headings: galaxies: Magellanic Clouds – interstellar: matter – stars: supernovae

1. Introduction

30 Doradus in the Large Magellanic Cloud (LMC) exhibits extremely active star formation and interstellar activity. It serves as an interesting laboratory for the study of the evolution of the interstellar medium (ISM) and its interaction with massive stars. Many giant HI sheets in this region were identified in deep $H\alpha$ photographs (Meaburn 1980) and in 21-cm emission (Meaburn et al. 1987). These shells enclose about ten interlocking superbubbles each about 100 pc in diameters and expanding at about 30 - 50 km s⁻¹. Emission and absorption lines (Smith & Weedman 1971; Canto et al. 1980; Cox & Deharveng 1983; Meaburn 1984; and Clayton 1987) revealed a complicated velocity structure which closely correlates with HI components. The observed components range over $V_{hel} = 185 - 307$ km s⁻¹. X-ray maps (Wang & Helfand 1991a, b) demonstrate a good correlation with $H\alpha$ images, indicating that these superbubbles contain hot gas. It was shown (McCray & Kafatos 1987) that repeated supernova explosions of massive stars play the major role in pressurizing these giant bubbles and evacuating interstellar space, culminating in 600-800 pc diameter supershells.

SN1987A in the LMC provided a unique opportunity for studying part of the 30 Doradus complex. [Ca II], Na D and UV absorption lines against SN1987A (Andreani, Ferlet & Vidal-Madjar 1987, Vidal-Madjar et al. 1987, Magain 1987, and Blades et al. 1988) exhibit groups of LMC components near $V_{hel} = 129, 171, 206, 226, 250-265$ and 281 km s⁻¹. These features indicate the presence of interstellar superbubbles, and are consistent with the results in other parts of 30 Doradus. Other studies (deBoer et al. 1990) indicate that the components with velocities less than 140 km s⁻¹ are not associated with the LMC (and are also weaker).

The study of this part of space was greatly boosted by the discovery of the light echoes from SN1987A (Crotts 1988). As forward scattered light from the SN, light echoes carry

information not only about the SN, but also about the interstellar dust which reflect them. In the decade since the first discovery, these light echoes from SN1987A have revealed a great deal of information about this region (Suntzeff et al. 1988; Gouiffes et al. 1988; Crotts, Kunkel & McCarthy 1989; Bond et al. 1989; Couch, Allen & Malin 1990; Xu, Crotts & Kunkel 1994; and Spyromilio et al. 1995). In a more recent paper (Xu, Crotts & Kunkel 1995), we discuss comprehensively the large scale ISM structures in the SN1987A foreground, and constructed a three-dimensional (3D) map of these complicated structures from the light echoes. Twelve dust sheets were identified: R310, R430, W700, S730, N980, R1170, SW1400, NW1500, W1700, R1830, SE3140, and N3240. These names are derived from the following rules: the first one or two letters indicate the direction relative to SN1987A, e.g. “R” for ring shaped, “N” for north and “SE” for south-east; the following number is the distance in front of SN1987A in light years. These structures enclose a 110 pc radius superbubble which interlocks with a smaller, 30 pc bubble, a 600 pc diameter giant superbubble, and a shell which likely envelopes SN1987A. The giant superbubble appears to have also been observed by another group (Bruhweiler, Fitzurka & Gull 1991) as an oval-shaped dust ring of 1.5-2.0 kpc in dimensions in a narrow continuum band (4215Å).

One of the important results from 3D light echo mapping is that the superbubble N157C is not just the smallest “cavity” enclosed by the H α filaments to the north-east of SN1987A (for example, see Meaburn 1980). Instead, the complicated H α structure which extends to the south-west of SN1987A, has a spherical 3D structure whose center of curvature falls on LH90. Therefore, we think that the N157C supershell extends to a radius of about 115 pc to the south-west, in the direction of SN1987A. An X-ray map (Wang & Helfand 1991a) reveals a bubble bigger than the small cavity which was believed to be N157C. The X-ray maps are likely to show where gas is hitting the inner surface of the shell, with gas interior to this probably too diffuse to detect. The lowest contour level (0.0013 photon s $^{-1}$ arcmin $^{-2}$) of the partial X-ray ring around the central OB association

LH 90 actually extends to a radius of about 60 pc (4.0 arcmin), but is incomplete to the south and west around its circumference. It appears that the N157C bubble extends to larger radii towards the west and south, towards the direction of the SN. In the deepest ROSAT PSPC images of the same field (Hasinger et al. 1996), it is clear that two segments of X-ray emitting gas, roughly concentric with respect to the center of N157C, sit in the region extending into our survey field, the farthest one at a radius of about 100 pc (~ 6.5 arcmin) with respect to N157C’s center. Future observations might reveal if these have the same spectrum as the rest of the X-ray shell. One cannot prove on the basis of X-ray morphology alone where the edge of the superbubble extends in the direction of the SN, but it seems likely to be larger than the 60 pc radius seen at other position angles. In contrast N157C seen in 21-cm emission from H I extends over at least 200 pc in diameter (Kim et al. 1998), nearly coextensive with the dust echo.

It is highly desirable to study the velocities of these structures. Echelle emission spectra in the vicinity of SN1987A were reported before (Meaburn 1990). The components were found consistent with absorption structures, with 255 and 280 km s⁻¹ the two most ubiquitous components. In this paper, we will present the results of our large field echelle survey around SN1987A and its relation to the ISM structures. Section 2 discusses observations and data reduction. Section 3 will explain our numerical model and fitting procedure. We interpret the velocity map in §4.

2. Observations and Data Reduction

The survey was conducted on 22-24 January 1993 and on 16-18 January 1994 using the Cassegrain echelle spectrograph on the CTIO 4m telescope. We used an echelle setup of five evenly spaced long slits, oriented north-south. The slits were 131'' long and centered 12''.5 apart from each other. With such five slits, every exposure covered a field of 131'' \times 50''.

By making the offset between fields $120''$ north-south and $60''$ east-west (hence $10''$ between adjacent exposures) there was sufficient overlap north-south to check that we had returned to the same right ascension on later nights (while the east-west offsets, also double-checked by occasionally re-acquiring the SN, were made in quick succession on the same night). We planned to use 18 such evenly distributed fields to cover a $370'' \times 350''$ region, from $125''$ south to $245''$ north of SN1987A, and from $170''$ west of to $180''$ east of SN1987A. We managed to get 17 fields, not having enough time to observe the south-westernmost corner field. Additionally, two single $247''$ -long slits oriented east-west, one centered on the SN and one centered $100''$ north of the SN, were also used beforehand to check for structure that might extend beyond the 120 km s^{-1} free velocity range between adjacent slits. No such structure was found, with the exception of a small region in the five-slit data at the edge of the field southeast from the SN. This corresponds to the “Honeycomb Nebula” (Wang 1992, Meaburn et al. 1993, Meaburn et al. 1995, Chu et al. 1995), where we ignored some data which appeared susceptible to overlap. The configuration of all of these slit positions is shown in Figure 1.

We chose to look at the [N II] doublet (air $\lambda 6548.08$ and $\lambda 6583.41$: Osterbrock, Tran, & Vielleux 1992), and used an $H\alpha$ filter (central wavelength = 6563\AA , FWHM= 75\AA) to separate orders. We use [N II] instead of $H\alpha$ because the thermal width of $H\alpha$ line is about 3.7 times of that of [N II] line at the same temperature due to the difference in their atomic mass, a critical difference. Resolution of the setup is 10 km s^{-1} near [N II] $\lambda 6583.41$, and the free velocity range between every two slits is 120 km s^{-1} . Exposure time of each field is 3600 seconds.

We used IRAF to reduce the data. The process started with column bias, two-dimensional bias frame subtraction, and dark current subtraction. Bad pixels were interpolated over. The response function image from each night, which was later used to

flat field the images, was constructed from combined quartz exposures using the IRAF “response” task. We then used the IRAF “illumination” task to fit “slit functions” from sky exposures. These slit functions were then applied in illumination correction to all the object images to give a flat response along slits. We calibrated the spectra into wavelength space using ThAr comparison spectra. The calibration error can be assessed by comparing the measured sky line wavelength to the standard values (Hubbard et al. 1986). We found the error was less than 0.04 \AA , or equivalently 2 km s^{-1} at $\lambda 6548$. This error is only $1/5$ of the 10 km s^{-1} resolution. Because the later process requires a high S/N ratio, we binned the spectra over every $13''.3$. A continuum was then fit and subtracted from each one of the $13''.3$ spectra. We then scaled the spectra in adjacent fields to the same flux level. The scaling was possible because we deliberately overlapped each field with its neighbors. We multiplied spectra of each field by a constant so that neighboring fields have the same $H\alpha$ and NII ($\lambda 6583$) flux in the common region. Finally, night sky lines were properly subtracted from the spectra. Unfortunately, one of the [N II] doublet ($\lambda 6548.08$) was terribly contaminated by OH-lines. Therefore, we only look at the other [N II] line $\lambda 6583.41$.

3. Velocity Components Analysis

We transformed the spectra into velocity space using the Doppler shift formula. The NII vacuum wavelength are $\lambda 6549.87$ and $\lambda 6585.21$ which are calculated from their air wavelengths with Edlen’s formula (Edlen 1966).

3.1. Component Identification

It is crucial to first identify structures corresponding to each slit, because the 5-slit echelle may cause cross-slit overlap. For this purpose, we looked at two single slit spectra: one centered on SN1987A, and the other about $100''$ to the north. We first binned them over $130''$ to achieve a high S/N level. Figure 2 show $H\alpha$ and $[N\ II]\lambda 6583$ lines of these spectra. In Panels 1 and 3 ($H\alpha$ line), the two structures near 0 and 650 km s^{-1} are skylines $\lambda 6562.67$ and $\lambda 6577.21$ (Hubbard et al. 1986) respectively. In Panels 2 and 4 ($[N\ II]\ \lambda 6583$ line), the structure near 600 km s^{-1} is a skyline $\lambda 6596.55$ (Hubbard et al. 1986). These spectra show that the only interesting structures are in $210\text{--}330\text{ km s}^{-1}$ interval, which is within our slit-to-slit free range. Although this conclusion is technically correct only in the region on and to the north of SN1987A, we think it is very unlikely that some extraordinary low or high velocity structure would appear only to the south of SN1987A, since most structures are seen to be weaker there.

3.2. Numerical Analysis

The goal of numerical analysis is to identify the number of velocity components and to measure the properties of each component, e.g. velocity, intensity and FWHM. Our analysis was a two-step process. We first fit the data with various numerical models with up to five gaussian components. Then based on the fitting result, we used a statistical algorithm to select the correct component numbers.

First, we varied the number of Gaussian components from one to five to produce five different models. These models were fitted separately to the spectra using least χ^2 fitting to determine the parameters. Because the temperature of each component in the LMC should not change very much, and hence the FWHM of each component should be roughly the

same, we forced a uniform FWHM across components within each model, while the height and position were allowed to vary freely and independently from each other. To check out the “uniform FWHM” assumption, we repeated the whole process but let FWHMs vary as free variables. The “model probability” method (see below) selected the same number of components in every field, regardless the assumption on FWHMs. We also noticed that the velocities of corresponding components are a little different, but within our resolution. Therefore, we think our modeling based on the “uniform FWHM” assumption is robust. The fitting was performed with the “deblend” option of IRAF’s “splot” task. We chose to work interactively because the components are normally not well separated and automatic fitting tends to yield wild results.

Based on the least χ^2 fitting result, we computed the probability that a “correct” model would yield a higher χ^2 than the actually fitted result. The selection rule is that the most likely model has the maximum probability. It has been shown that the probability defined in this way satisfies a χ^2 -distribution and consequently can be calculated (Press et al. 1992). For every profile, we compared the five models based on their probabilities, and select the one with the highest probability. In most cases, we found the “correct” model yields a probability several orders of magnitude higher than other models, and hence convincingly establishes itself. For a few profiles, two or three models have similar probabilities. In these situations, we made our choices by continuity argument. We look at the neighboring locations for any definitely “correct” models, and select the most similar one. Figure 3 shows the reduced data from one of our 17 fields, detailing the [N II] λ 6583 line, and the result from our velocity component analysis graphed on a corresponding scale in the adjacent diagram. The analysis reveals all of the major features and nearly all weaker ones, and follows gradients in the velocities of components with reasonable accuracy.

With the aforementioned process, we determined at every grid point over all 17 fields

the number of components and properties of each component. We then looked into the connection among these grid points for collective structures across the field. The result will be discussed in the next section.

4. ISM in the Foreground of SN1987A

This survey shows the following ionized clouds: $V_{hel} = 237, 245, 255, 265, 277, 285, 300$, and 313 km s^{-1} . (When clouds are within about 5 km s^{-1} of each other, they tend to blend together.) These are shown in Figure 4a. The $265 - 285 \text{ km s}^{-1}$ grouping is sufficiently complex that we show it separately in Figure 4b. Four of these components (255, 277, 300 and 313) were also reported in a smaller field containing SN1987A (Meaburn 1990). Two of them, $V_{hel} = 255$ and 277 km s^{-1} were discovered in the interstellar absorption spectra toward SN1987A (see the citations in §1). A HI 21-cm study in this region exhibited similar profiles: $V_{hel} = 243, 274, 296$ and 318 km s^{-1} (Meaburn, McGee & Newton 1984). Similar structures were also discovered in the halo of 30 Doradus from [O III] lines (Meaburn 1984; Meaburn 1988). In our survey, we found the 245 and 255 km s^{-1} components (Group B in Figure 4a) have similar properties and hence are likely to be two layers of one structure (see §4.3 below). Similarly, $V_{hel} = 265, 277$ and 285 km s^{-1} clouds (Group C and Figure 4b) are seen to be interrelated with each other and even connected in some places. (Some components are seen to disappear into others when approach within the 5 km s^{-1} blending range.) We think these three are really one structure (see §4.1 below). The two high velocity clouds (300 and 313 km s^{-1} ; Group D) are likely to be the far side of the $245\text{-}255 \text{ km s}^{-1}$ shell (§4.3, see also Meaburn 1990). The other component (237 km s^{-1} ; Group A) is reported for the first time in this study. It is interesting that we did not see this component in the two single long slit spectra, one centered on SN1987A and the other $100''$ north of the supernova. We show in §4.2 that this component correlates to the two

clouds about 1 kpc in front of SN1987A (Xu, Crofts & Kunkel 1994).

4.1. N157C

The $V_{hel} = 265, 277$ and 285 km s^{-1} group (C in Figure 4a, also seen in Figure 4b) is the most far reaching structure in this field. They not only are interrelated with each other, but also have comparable flux level consistently bright throughout the whole field. Similar behavior was observed in [OIII] and $H\alpha$ emission lines (Meaburn 1990), in the HI 21-cm survey (Meaburn, McGee & Newton 1984), and in [Ca II], Na D and UV absorption lines (see §1 for references). Therefore, it is tempting to recognize these three components as one dominant structure in front of SN1987A. In an earlier paper (Xu, Crofts & Kunkel 1995), we show that the most prominent structure in the SN foreground is the echo 1170 light-years in the SN foreground, the R1170-complex (identified as N157C). This similarity marks the first correlation indicating that these velocity components are indeed N157C.

As another piece of evidence, we plotted the flux contour of these components on top of the 2D image of the ISM dust structure, the R1170-complex (Xu, Crofts & Kunkel 1995) (Figure 5). This plot shows a general tendency that both structures are bright to the north of SN1987A. In addition, we observed a good correlation not only on the large scale but also at many small bright spots, limited by the spatial accuracy of the echelle survey of $13''$ east-west and $40''$ north-south.

We also observed that the two structures split in the same way. The 3D light echo map (Xu, Crofts & Kunkel 1995) demonstrated that the cloud, consisting of N1500 and W1700, splits from R1170 to the north of SN1987A and joins R1830 southwest of the SN. Similarly, Figure 4b shows the 277 km s^{-1} component joining the 285 km s^{-1} component to the south (and slightly east) of SN1987A and the 265 km s^{-1} component to the southwest.

This geometry is consistent with the picture that the 285 and the 265 km s⁻¹ components are the far and near shell of N157C, while the 277 km s⁻¹ component is a cloud joining the two structures to form a superbubble.

N157C, with a diameter of about 200 pc, is expanding at a speed of 10 km s⁻¹, therefore. We believe this bubble is still in the pressure-driven stage for the following reasons. First, this size is common in other parts of the LMC, particularly in 30 Doradus (Meaburn 1980). Most of these giant bubbles are young and rapidly expanding (Meaburn et al. 1987). McCray and Kafatos (1987) attributed the generally large superbubble size to the thick gas disk of the LMC and its low metallicity. Secondly, the interior of a pressure-driven bubble is filled with hot gas as opposed to the cool interior in the snow-plow stage. In addition, Wang and Helfand (1991b) reported X-ray ($\approx 0.8 - 1.2 keV$) emission in N157C, corresponding to very hot gas in its interior. Therefore, N157C is in the energy-conservation stage. McCray and Kafatos (1987) gave the radius and velocity properties for these bubbles:

$$R_S = 97 \text{ pc } (N_\star E_{51}/n_0)^{1/5} t_7^{3/5} \quad (1)$$

$$V_S = 5.7 \text{ km s}^{-1} (N_\star E_{51}/n_0)^{1/5} t_7^{-2/5} \quad (2)$$

Dividing one equation by the other,

$$t_7 = \frac{R_S}{V_S} \frac{5.7 \text{ km s}^{-1}}{97 \text{ pc}} \quad (3)$$

where n_0 is the gas atomic density, and $t_7 = t/10^7$ yr. Let $R_S = 100$ pc, $V_S = 10$ km s⁻¹. We estimate the age of N157C to be $t = 6$ Myr. Therefore, this superbubble is still very young. It is estimated (McCray & Kafatos 1987) that stellar winds from a rich cluster ($N_\star \geq 10$) dominate its superbubble expansion for a few million years until supernova explosions become more important, while the superbubble may expand to less than ≈ 100 pc. We think N157C has just passed the stellar-wind-driven stage, and is in rapid expansion driven by powerful supernovae from LH90.

From other sources, we estimate the neutral hydrogen column density N_{HI} of the supershell N157C. From 21 cm emission (Luks & Rohlfs 1992), about 70% of the H I column density towards LH90 is contained in a narrow component centered at 270 km s⁻¹, with a total column density of all components of about 2.2×10^{21} cm⁻². This total N_{HI} is corroborated from the pointing (#43) containing N157C from the survey of Meaburn et al. 1987: $N_{HI} = 2.3 \times 10^{21}$ cm⁻², and the value inferred from the extinction of the star Sk -69°203, in the direction of N157C: 2.4×10^{21} cm⁻² (Fitzpatrick & Walborn 1990). Thus the value of N_{HI} for N157C is about 1.5×10^{21} cm⁻². (However, none of these surveys have resolution better than about 15', so we cannot be sure of the effects of substructure.) Since this column density is optically thick at the Lyman limit, we will assume the gas is shielded and therefore largely neutral. Accounting for projection effects (a factor of four), the kinetic energy of the expanding HI shell is therefore $E_{shell} = 5.4 \times 10^{50}$ ergs. This implies a total kinetic output from SNe that is 77/15 times greater (Mac Low & McCray 1988): $E_S = 2.7 \times 10^{51}$ ergs. Each typical Type II supernova of a massive O star releases about $E_{SN} = 10^{51}$ ergs of kinetic energy. Given an average supernova rate of about one per million years in a typical OB association (Mac Low & McCray 1988), the energy budget is consistent with the aforementioned age estimate.

Given E_{shell} determined from theoretical consideration of a SN driven expansion (McCray & Kafatos 1987):

$$E_{shell} = 4.0 \times 10^{49} \text{ ergs } (N_{\star} E_{51}) t_7 \quad (4)$$

we find $N_{\star} E_{51} = 22$. Combining this with Equation 1 (or 2) yields an initial density $n_0 = 4$. This is a reasonable estimate, corresponding to the $N_{HI} = 2.4 \times 10^{21}$ cm⁻² spread over a scale height of 100 pc, which is reasonable in terms of the observed 3-D structure.

On the other hand, from stellar content point of view, the aforementioned estimate $N_{\star} E_{51}$ implies several massive SN explosions in LH90, given that the typical energy of a

Type II SN, E_{51} , is a few for the most massive stars ($M \geq 30M_{\odot}$). The main-sequence lifetimes of massive stars are given approximately by $t_{MS} \approx 30 \text{ Myr } (M_{\star}/[10M_{\odot}])^{-\alpha}$, where $\alpha \approx 1.6$ for $7 \leq M_{\star} \leq 30M_{\star}$ (Stothers 1972) and by $t_{MS} \approx 9 \text{ Myr } (M_{\star}/[10M_{\odot}])^{-0.5}$ for $30 \leq M_{\star} \leq 80M_{\star}$ (Chiosi, Nasi & Sreenivasan 1978). In a time scale of 6 Myr, only a few very massive stars with ($M_{\star} \gtrsim 30M_{\odot}$) would explode. It is estimated that an OB association should produce roughly 9 times as many stars with masses in the range 7-30 M_{\odot} (main-sequence spectral type B3-08, corresponding to N_{\star}) as stars with masses $\geq 30M_{\odot}$ (MS type O7-03) (McCray & Kafatos 1987). Given that there are about 50 stars with mass $\geq 7M_{\odot}$ (Hill et al. 1994), there should be about 5 massive stars of $M_{\star} \gtrsim 30M_{\odot}$ which should have exploded.

We can also compare our predicted SN explosion number to empirical determinations of the stellar population. In addition to the original study of LH 90 (Lucke & Hodge 1970), two recent studies of the stellar population of the association yield somewhat different results. Recent UIT data (Hill et al. 1994) on LH90 and six other LH OB associations in all but the inner portion of the 30 Dor complex give the number of stars and their inferred mass. For the clusters with the largest mass stars ($\approx 50M_{\odot}$), the ratio of $M \geq 30M_{\odot}$ versus $7M_{\odot} \geq M \gtrsim 30M_{\odot}$ stars predicted in the previous paragraph from theoretical estimations appears inconsistent with the UIT data, in the sense that more massive stars are actually seen by UIT. From these data, LH90 appears to have stars as massive as $41M_{\odot}$, while LH89 and LH99 show about eight stars more massive than this (out of a total of 40 stars in LH90 and 68 stars in LH89 and LH99 more massive than $15M_{\odot}$). Thus LH90 might be missing approximately five stars of $M \approx 50M_{\odot}$ (or more if stars have exploded in LH89 or LH99); these have presumably formed SNe.

We should note, however, the existence of stars in LH90 more massive than those allowed ($\gtrsim 30M_{\odot}$) by a 6 Myr year turnoff age. Perhaps some massive stars were created

millions of years after the first stars. Indeed, our prediction for the number of massive stars seems more consistent with the results from the other study (Testor et al. 1993), which uses optical photometry and spectroscopy of LH 90 to derive spectral types and M_{bol} values consistent with about 7 stars with $M_{\star} \gtrsim 30M_{\odot}$ versus more than 47 stars with mass $\geq 7M_{\odot}$ (according to our simple conversion of M_{bol} to M_{\star}). Indeed, their study concludes that the association contains a sub-population 3-4 Myr old and a possible larger sub-population 7-8 Myr old (Testor et al. 1993). This is consistent with our arguments regarding the SN rate.

4.2. 600 pc Giant Superbubble

Xu, Crofts and Kunkel (1994) first reported two dust bodies at about 1 kpc in front of SN1987A. They (Xu, Crofts & Kunkel 1995) also found that the southeast piece of these two correlates with one of the bright $H\alpha$ filaments extending from N157C discovered by Meaburn (1984). They went one step further to suggest this filament as the near side and N157C as the far side of a giant superbubble of 600 pc in diameter. Consistent with this picture, a component at 235 km s^{-1} (“A” in Figure 4a) has been found in the regions far away from SN1987A. Figure 6 plots flux contour of this component over the image of SE3140 and N3240 (Xu, Crofts & Kunkel 1995). We found that one piece of the 235 km s^{-1} components corresponds exactly to N3240, and another piece correlates with SE3140. It is unfortunate that we only had enough time to finish the survey to the north of Dec $-69^{\circ}18'$ and to the west of RA 5h 36m 00s (in J2000) delineated by the dashed lines. Still, the available data indicates that 235 km s^{-1} gives a good correlation with SE3140, expanding at about 40 km s^{-1} relative to the centroid of N157C.

It is interesting to see the 235 km s^{-1} component distributed in a patchy ring-like shape. Recent light echo images (1995-1997) showed N3140 becoming larger and extending

to the position angle $PA = 45^\circ$ where the $(5h36m, -69^\circ14')$ 235 km s^{-1} components is located. Therefore, we think the 1 kpc ISM structure may indeed show a hole in front of SN1987A. Moreover, we have several reasons to believe this hole may relate to the blow-out of the 600-pc-diameter superbubble. First, we have not observed any structure within $3'$ of SN1987A either in the light echoes at 1 kpc or in the echelle survey at 235 km s^{-1} , indicating that the cloud has been fragmented. This result can be explained by a superbubble blow-out. Secondly, Wang and Helfand (1991b, c) reported that this region has soft X-ray emission much higher than the background but much lower than other young superbubbles in 30 Doradus. This region may even be contained in the possible giant superbubble LMC-2, roughly 1 kpc across (Wang & Helfand 1991c) which has blown out of the disk. Finally, 600 pc is one of the largest superbubbles ever observed in the LMC (Meaburn 1980), and therefore may represent a size close to the upper limit imposed on the superbubble size by the LMC disk thickness. In conclusion, we think this 600 pc diameter giant superbubble appears to have blown out of the LMC disk and is expanding in radius (assuming it is pushing on one side against N157C) at 20 km s^{-1} . McCray and Kafatos (1987) suggested that when the superbubble cools or breaks out of the galaxy, it will be distorted by gravitational instability, collapse and form giant clouds, and finally ignite propagating star formation. LH90, which formed N157C, may have itself formed in this way in the gravitational collapse of the 600 pc giant bubble.

If this superbubble blew out in its snow-plow stage, prior to this it was described in terms of the time (t_c) and expansion radius (R_c) beyond which cooling becomes important in the interior e.g. post-adiabatically according to (McCray & Kafatos 1987):

$$R(t) \approx R_c(t/t_c)^{1/4} \quad (5)$$

for

$$R_c = 50 \text{ pc } \zeta^{-0.9} (N_\star E_{51})^{0.4} n_0^{-0.6} \quad (6)$$

and

$$t_c = 4 \times 10^6 \zeta^{-1.5} (N_\star E_{51})^{0.3} n_0^{-0.7} \quad (7)$$

where ζ is metallicity, N_\star is number of stars $\geq 7M_\odot$, $E_{51} = E/10^{51} \text{ ergs}$, n_0 is gas atomic density. In the LMC, $\zeta \approx 0.3$ (Dufour 1984) and a density typical for the LMC (several times lower than near N157C), $n_0 \approx 0.35$ (Hindman 1967). Let's guess $N_\star = 50$ (roughly that of N157C) and $E_{51} = 1$, hence $t_c = 160$ Myr, and $R_c \approx 1.3$ kpc, much bigger than 300 pc. Therefore, we think this giant bubble was probably hot when it blew out, implying an age at the time of blowout of about 10 Myr from eq. 3, or 15 Myr using eq. 1 and the (less certain) parameters above. These are probably consistent with the age of LMC-2 (Wang & Helfand 1991c). This appears older than N157C, indicating the 600 pc superbubble predates it, and may have even brought about LH90's formation.

4.3. Interstellar Environment of SN1987A

Xu, Crotts & Kunkel 1995 demonstrated that the two dense clouds (R430-complex including R310) about 100 pc in front of SN1987A do not correspond to any prominent $H\alpha$ structures, and therefore are likely related primarily to SN1987A. R430 is brighter and larger than R310. The lack of correlation is also consistent with the assertion that SN1987A exploded about 300 pc on the far side of the LMC disk (Xu, Crotts & Kunkel 1995). Figure 7 plots flux contour of $V_{hel} = 255$ and 245 km s^{-1} (Group B in Figure 4a) on top of R430-complex, indicating a good correlation between these two images. On the other hand, the 255 km s^{-1} component is brighter and larger than 245 km s^{-1} component, in good agreement with the relative size and brightness of R430 and R310. The correlation between these two studies indicates that the double shell structure R430 and R310 have velocities 255 km s^{-1} and 245 km s^{-1} respectively. The 255 km s^{-1} component was reported by other groups before (see Meaburn 1990 and the reference therein). However, Meaburn

(1990) suggested that the 255 km s^{-1} shell is within 10 pc of SN1987A.

Two other ionized clouds $V_{hel} = 300$ and 313 km s^{-1} in the echelle spectra (Group D in Figure 4a) do not correspond to any absorption structures. It was suggested (Meaburn 1990) that these two clouds are likely to be the far side of a superbubble which envelops SN1987A. We noticed that this identification is consistent with the double shell structure on the near side. Unfortunately, the light echoes have expanded to only several light years behind SN1987A. So far, we do not have any direct light echo results on these two possible double shells on the far side of the supernova. Therefore, we can only speculate on the structures of these two high speed components.

If these two components are indeed on the far side of a superbubble surrounding SN1987A, this superbubble is expanding in radius at 30 km s^{-1} . If we adopt a average radius of 90 pc, the age of this bubble is about 2 Myr, (eq. 1). Let the shell density of this bubble $N_H \approx 1 \times 10^{20}$ (Meaburn et al. 1987), using the same method in §4.1, we calculate the total energy of this superbubble to be 3×10^{51} ergs, which is the energy of two to three typical Type II supernovae. Both the energy budget and the age suggest that there had been a small number of supernova explosions before SN1987A in this superbubble. Because of the short lifetime of this bubble, these previously exploded supernovae must be very massive stars ($M_{\star} \geq 30M_{\odot}$) (Chiosi, Nasi & Sreenivasan 1978).

The aforementioned superbubble assertion has some problems. First, there are not many stars close to SN1987A. Even though one may argue that massive stars might have exploded, the lack of low mass stars is still a difficulty. Second, the expansion velocity of 30 km s^{-1} is too high compared to that of N157C (10 km s^{-1}) which is pressurized by the second richest cluster LH90. The only way around this problem is to assume very low gas density in this region. In Equation 2, adopt $V_S = 30 \text{ km s}^{-1}$, $N_{\star}E_{51} = 3$, $t_7 = 0.2$, we get $n_0 = 0.02$, which is an order of magnitude lower than the typical LMC value of $n_0 = 0.35$

(Hindman 1967). Perhaps this is reasonable, given SN1987A’s likely distance from the plane of the LMC, but the existence of a superbubble surrounding SN1987A is still not certain.

We also noticed that there are two components at 269 and 301 km s^{−1} within 20'' of SN1987A. They have much higher flux level than those probably more distant components at 245, 255 and 317 km s^{−1} (and at 300 km s^{−1} not within 20''). It has been suggested that these structures are probably due to the emission from the red supergiant wind (Crotts & Kunkel 1991). This structure will be treated in a separate paper (Crotts & Heathcote 1998). These two components have been reported previously (Meaburn 1990).

5. Discussion

We note that our light echo 3-D map, in conjunction with the velocities of the matter in front of the SN from this study, implies that the SN is well behind most of the material in its portion of the LMC, and hints at how this occurred. This refutes claims made on the basis of extinction towards a nearby star, Sk −69°203, that the SN is embedded in the middle of the main H I complex (Fitzpatrick & Walborn 1990). We approximate the speed of LH90 with that of N157C, about 270 km s^{−1}. This should also represent the speed of the LMC stellar disk. Therefore, SN1987A is moving away from the LMC disk at a speed of 20 km s^{−1} given that the velocity of SN1987A of 289 km s^{−1} (Crotts & Heathcote 1991). At this speed, it would have taken the SN1987A progenitor $\sim 10^7$ years to move to its current location 300 pc away from the stellar disk. It is interesting to compare this time scale to the lifetime of N157C (6 Myr, §4.1) as well as that of the speculated superbubble surrounding SN1987A (2 Myr, §4.3), and that of the progenitor itself. We speculate that the SN and N157C were created together (followed by the superbubble around SN 1987A), and are pursuing further methods to test this.

The authors would like to thank Cerro Tololo Inter-American Observatory for granting observing time to this study and all the wonderful support that we have received. We would also like to direct our gratitude to Rob Olling and David Helfand for many enlightening discussions. This research was supported by NSF grant AST 90-22586, the A.C.'s David & Lucile Packard Foundation fellowship, and NASA LTSA grant NAG5-3502.

REFERENCES

- Andreani, P., Ferlet, R., and Vidal-Madjar, A., 1987, *Nature*, 326, 770
- Blades, J.C., Wheatley, J.M., Panagia, N., Grewing, M., Pettini, M., and Wamsteker, W., 1988, *ApJ*, 334, 308
- Bond, H.E., Panagia, N., Gilmozzi, R., and Meakes, M., 1989, *IAU Circular*, 4733
- Bruhweiler, F.C., Fitzurka, M.A., and Gull, T.R., 1991, *ApJ*, 370, 551
- Canto, J., Elliott, K.H., Goudis, C., Johnson, P.G., Mason, D., and Meaburn, J., 1980, *A&A*, 84, 167
- Chiosi, C., Nasi, E., and Sreenivasan, S.P., 1978, *A&A*, 63, 103
- Chu, Y.-H., Dickel, J.R., Staveland-Smith, L., Osterberg, J., and Smith, R.C., 1995, *AJ*, 109, 4
- Clayton, C.A., 1987, *A&A*, 173, 137
- Couch, W.J., Allen, D.A., and Malin, D.F., 1990, *MNRAS*, 242, 555
- Cox, D.P., and Deharveng, L., 1983, *A&A*, 117, 265
- Crotts, A.P.S., 1988, *ApJ*, 333, L51
- Crotts, A.P.S., Kunkel, W.E., and McCarthy, P.J., 1989, *ApJ*, 347, L61
- Crotts, A.P.S., 1990, *ESO/EIPC Workshop “SN1987A and Other Supernovae”*, ed. J. Danziger (ESO Garching), p. 559
- Crotts, A.P.S., and Kunkel, W.E., 1991, *ApJ*, 336, L73
- Crotts, A.P.S., and Heathcote, S.R., 1991, *Nature*, 350, 683

- Crotts, A.P.S., and Heathcote, S.R., 1998, in preparation
- deBoer, K.S., Morras, R., and Bajaja, E., 1990, *A&A*, 233, 523
- Dufour, R.J., 1984, in *IAU Symposium 108, Structure and Evolution of the Magellanic Clouds*, ed S. van den Bergh and K.S. de Boer (Dordrecht: Reidel), p. 353.
- Edlen, B., 1966, *Metrologia*, 2, 71
- Fitzpatrick, E.L., and Walborn, N.R., 1990, *AJ*, 99, 1483
- Gouiffes, C., et al., 1988, *A&A*, 198, L9
- Hasinger G., Aschenbach, B. and Trümper, J., 1996, *A&A*, 312, L9
- Hill, J. et al., 1994, *ApJ*, 425, 122
- Hindman, J.V., 1967, *Australian J. Phys.*, 20, 147
- Hubbard, et al., private communication, 1986
- Kim, S., Staveley-Smith, L., Dopita, M.A., Freeman, K.C., Sault, R.J., Kesteven, M.J., and McConnell, D. 1998, *ApJ*, 503, 674
- Lucke, P.B., and Hodge, P.W., 1970, *AJ*, 75, 171
- Luks, T., and Rohlfs, K., 1992, *A&A*, 263, 41
- Mac Low, M.M., and McCray, R., 1988, *ApJ*, 324, 776
- Magain, P., 1987, *Nature*, 329, 606
- McCray, R., and Kafatos, M., *ApJ*, 317, 190
- Meaburn, J., 1980, *MNRAS*, 192, 365

- Meaburn, J., 1984, MNRAS, 211, 521
- Meaburn, J., 1988, MNRAS, 235, 375
- Meaburn, J., 1990, MNRAS, 244, 551
- Meaburn, J., McGee, R.X., and Newton, L.M., 1984, MNRAS, 206, 705
- Meaburn, J., Marston, A.P., McGee, R.X., Newton, L.M., 1987, MNRAS, 225, 591
- Meaburn, J., Wang, L., and Bryce, M., 1995, A&A, 293, 532
- Meaburn, J., Wang, L., Palmer, J., and Lopez, J.A., 1993, MNRAS, 263, L6
- Osterbrock, D.E., Tran, H.D., and Vielleux, S., 1992, ApJ, 389, 308
- Press, W.H., Teukolsky, S.A., Vetterling, W.T., and Flannery, 1992, Numerical Recipes, (Cambridge U. Press), p. 653.
- Smith, M.G., and Weedman, D.W., 1971, ApJ, 205, 762
- Spyromilio, J., Malin, D.F., Allen, D.A., Steer, C.J., and Couch, W.J., 1995, MNRAS, 274, 256
- Stothers, R., 1972, ApJ, 175, 431
- Suntzeff, N.B., Heathcote, S., Weller, W.G., Caldwell, N., Huchra, J.P., Olowin, R.P., and Chambers, K.C., 1988, Nature, 334, 135
- Testor, G., Schild, H. and Lortet, M.C., 1971, A&A, 280, 426
- Vidal-Madjar, A., Andreani, P., Cristiani, S., Ferlet, R., Lanz, T., and Vladilo, G., 1987, Nature, 326, 770
- Wang, L., 1992, ESO Messenger, 69, 34

Wang, Q., and Helfand, D.J., 1991a, ApJ, 370, 541

Wang, Q., and Helfand, D.J., 1991b, ApJ, 373, 497

Wang, Q., and Helfand, D.J., 1991c, ApJ, 379, 327

Xu, J., Crofts, A.P.S., and Kunkel, W.E., 1994, ApJ, 435, 274

Xu, J., Crofts, A.P.S., and Kunkel, W.E., 1995, ApJ, 451, 806

Figure Legends

Figure 1: A $15'$ field centered on SN 1987A imaged in a band highlighting $H\alpha$ and $[N II]$, and showing the positions of our echelle long slits relative to features in the field. The OB association LH90 sits near the corresponding label, with the most prominent groups of stars seen to the west and south of the label. It is surrounded at radii out to $\sim 10'$ by emission from gas associated with the accompanying supershell N157C. The Honeycomb Nebula (labeled “HN”) sits about $2.5'$ southeast of the SN. At the time of these observations, the light echoes extended to roughly the edge of our slit array.

Figure 2: Binned spectra of two single $120''$ long slits. From upperleft counterclockwise are Panels 1, 2, 3 and 4. Panel 1: $H\alpha$ spectrum centered on SN1987A; Panel 2: $[N II]$ ($\lambda 6583$) spectrum centered on SN1987A; Panel 3: $H\alpha$ spectrum $100''$ north of SN1987A; Panel 4: $[N II]$ ($\lambda 6583$) spectrum $100''$ north of SN1987A. The abscissa is V_{hel} in km s^{-1} . The ordinates are in counts of each pixel. In Panels 1 and 3, the structures near 0 and 650 km s^{-1} are night sky lines. In Panels 2 and 4, the structures at 600 km s^{-1} are also night sky lines.

Figure 3a: The reduced data from one of our 17 subfields (the one just northwest of the SN). The range of data is 120 arcsec in the vertical direction (along the slit), with a free velocity range of 120 km s^{-1} corresponding to each of the five slits in the horizontal direction. The SN itself is seen in $[N II]\lambda 6583$ in the lower (southern) left corner.

Figure 3b: On the same scale as Figure 3a, the inferred velocity components are shown for the same data. The emission strength of each component (slit into 13.3 arcsec subsamples) is indicated by the width of each line segment, which varies with the logarithm of linestrength. The tickmarks along the vertical axis indicate divisions of 13.3 arcsec and those along the horizontal indicate steps of 50 km s^{-1} (in the frame of a single slit).

Figure 4a: 3-D surface plot of all eight velocity components in front of SN1987A. They are collected into four groups, A, B, C and D (described in §4), with labels of each letter at the corners of each group indicating its approximate extent on the plot. The vertical axis is V_{hel} in km s^{-1} . The other two axis are RA and Dec in J2000. North is to the left. West is the direction pointing into the paper. Note that structure within about 5 km s^{-1} will blend by one of them disappearing.

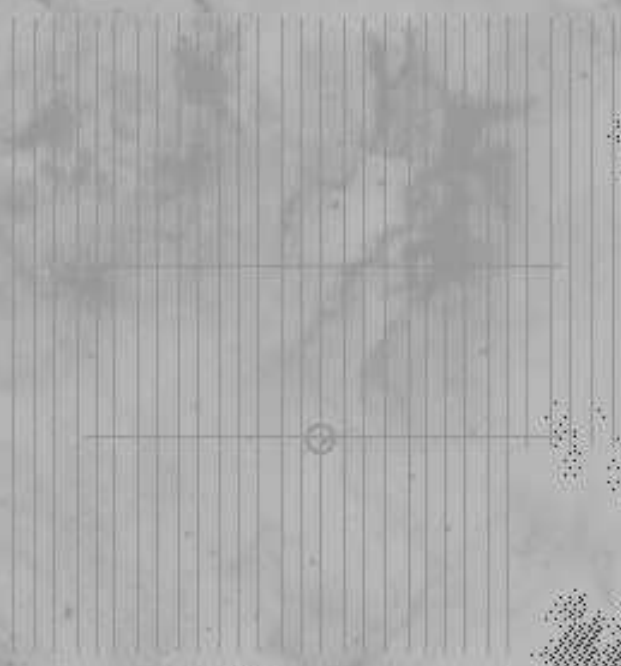
Figure 4b: 3-D surface plot of the three velocity components in Group C, 265, 277 and 285 km s^{-1} . The axes and orientation are the same as in Figure 4a. Notice that the 277 km s^{-1} component joins the 265 km s^{-1} component to the southeast of SN1987A, and the 285 km s^{-1} component to the south and slightly east of the SN.

Figure 5: Flux contour of combined $V_{hel} = 265, 277$ and 285 km s^{-1} components on top of the R1170-complex image (Xu, Crofts & Kunkel 1995). The axes are RA and Dec (J2000). Both the flux- and the dust-maps are smoothed in both directions over $13''$, which is the resolution limit of the echelle survey. This survey only covered the region within the dashed lines. The “holes” in the gray scale dust-map are due to the lack of data and inadequate contrast in image display after smoothing. The readers are encouraged to compare this plot and Figures 6 and 7 with the similar plot in Xu, Crofts & Kunkel 1995.

Figure 6: Flux contour of the $V_{hel} = 235 \text{ km s}^{-1}$ components plotted over the combined SE3140 and N3240 signals in greyscale (Xu, Crofts & Kunkel 1995), analogously to Figure 5.

Figure 7: As in Figure 5 and 6, flux contour of combined $V_{hel} = 245$ and 255 km s^{-1} components plotted over greyscale image of the R430-complex (Xu, Crofts & Kunkel 1995).

LH 90



HN



